Domain-Decomposed Lagrangian Data Assimilation for Drifting Sea-Ice Floe Dynamics

Danyang Li[1][0009−0007−0539−8029], John Taylor[2][0000−0001−9003−4076], and Quanling Deng[3,4][0000−0002−6159−1233]

[1] School of Computing, Australian National University, Canberra, Australia
Danyang.Li@anu.edu.au
[2] School of Computing, Australian National University, Canberra, Australia
John.Taylor@anu.edu.au
[3] Yau Mathematical Sciences Center, Tsinghua University, Beijing, China
qldeng@tsinghua.edu.cn
[4] School of Computing, Australian National University, Canberra, Australia
Quanling.Deng@anu.edu.au

Abstract. Sea ice dynamics are crucial to the global climate system, yet traditional continuum (e.g., viscous–plastic) models often fail to represent the discrete floe interactions that dominate in the marginal ice zone. Lagrangian discrete element methods (DEMs) resolve floe-scale physics more realistically, but their high particle counts make ensemble data assimilation (DA) more expensive. We consider a highly-simplified floe model and propose a scalable, domain-decomposed DA framework that couples Lagrangian particle observations with an ensemble transform Kalman filter (ETKF) to recover the underlying ocean flow field in a multiscale setting. The Eulerian domain is first partitioned into subdomains. We then impose an ETKF in each subdomain to recover the local fine-scale ocean features. A Gaussian-weighted blending step then reconstructs a globally consistent flow field across subdomain boundaries. Numerical experiments demonstrate consistently better skill scores that are characterised by normalised root mean square error (NRMSE) and pattern correlation coefficients (PCC), compared to the global and expensive DA baseline. Results suggest that the domain-decomposed DA method is an alternative, scalable approach for particle-based sea-ice floe dynamics and ocean flow recovery.

Keywords: sea ice dynamics · Lagrangian data assimilation · domain decomposition · ensemble transform Kalman filter

1 Introduction

Sea ice is a critical regulator of global climate and ocean circulation [21, 22, 32, 31]. At regional scales (>100 km), sea ice drift is primarily driven by wind stress and ocean forcing [8, 26]. While continuum models effectively reproduce large-scale motion [3, 16, 18, 24], they often homogenise floe-scale mechanics that dominate below ∼10 km [5, 14, 30]. With improving satellite products (e.g., SAR)

ICCS Camera Ready Version 2026
To cite this paper please use the final published version:
DOI: 10.1007/978-3-032-29912-3_8

resolving features at ∼km scale [8], particle-resolving approaches are increasingly feasible.

Lagrangian Discrete Element Methods (DEMs) evolve individual floes via Newton's equations and contact mechanics [9, 15, 17], enabling mechanistic representation of collision-driven dissipation, fracture, and floe-size redistribution [9, 20]. However, their cost grows rapidly with floe count, limiting applications to relatively small domains and idealised settings [15].

Data assimilation (DA) improves state estimation by combining observations with model dynamics [23]. In floe modelling, DA can adjust initial states and/or forcings to match observed Lagrangian trajectories [6, 7, 10]. Ensemble methods like the ensemble transform Kalman filter (ETKF) are used to handle nonlinear evolution and capture uncertainty [2, 12, 27]. Yet, scaling ETKF to DEM systems remains challenging due to high-dimensional states and dense observations.

Domain decomposition (DD) scales large numerical problems by splitting the domain into subdomains and solving coupled local problems [11, 29, 33], it have also been explored in ensemble DA to enable parallel updates[28]. Building on these developments, we propose a DD strategy for assimilating sparse Lagrangian observations in sea-ice dynamical systems. We partition the Eulerian domain into non-overlapping subdomains and run ETKF within each, assimilating only based on in-subdomain floe observations.Unlike fixed-radii localisation [19], which may truncate long-range correlations in particle systems, we blend the updated subdomain fields using a Gaussian-weighted average to obtain a coherent global velocity field and suppress boundary artefacts.

The rest of the paper is organised as follows. Section 2 formalises the problem and modelling assumptions. Section 3 presents the subdomain ETKF, floe selection, and Gaussian-weighted fusion. Section 4 reports NRMSE, PCC, and wall-clock runtime. Section 5 concludes and discusses limitations and future work.

2 Particle model for free-drifting floe dynamics

We adopt an idealised Lagrangian DEM to describe floe dynamics [6, 7]. Following standard practice [15, 9], each floe is represented as a cylinder of radius r and thickness h. Consider a system of L floes indexed by $l = 1, 2, \ldots, L$. The position and velocity of floe l are denoted by $\mathbf{x}_l$ and $\mathbf{v}_l$, and its mass, radius, and angular velocity are denoted by m_l, r_l, and ω_l, respectively. For simplicity, we focus on the dynamics of non-rotational free-drifting (thus non-collisional) floes. The modelling equations of motion follow Newton's second law and drag-forcing law:

$$\frac{d\mathbf{x}_l}{dt} = \mathbf{v}_l, \tag{1a}$$

$$m_l \frac{d\mathbf{v}_l}{dt} = \alpha_l(\mathbf{u}^o - \mathbf{v}_l)|\mathbf{u}^o - \mathbf{v}_l|, \tag{1b}$$

$$d\hat{\mathbf{u}}^o = (\mathbf{L}^{\mathbf{u}}\hat{\mathbf{u}}^o + \mathbf{F}^{\mathbf{u}})dt + \mathbf{\Sigma}^{\mathbf{u}} d\mathbf{W}^{\mathbf{u}}, \quad \mathbf{u}^o = \mathbf{G}(\mathbf{x})\hat{\mathbf{u}}^o, \tag{1c}$$

where $\boldsymbol{f}_l := \alpha_l(\mathbf{u}^o - \mathbf{v}_l)|\mathbf{u}^o - \mathbf{v}_l|$ is the ocean drag force following the quadratic law, $\mathbf{u}^o$ is the ocean field, and $\hat{\mathbf{u}}^o$ is corresponding Fourier modes of the ocean.

ICCS Camera Ready Version 2026
To cite this paper please use the final published version:
DOI: 10.1007/978-3-032-29912-3_8

Herein, we consider a one-way coupling in which a prescribed ocean current drives floe dynamics without feedback. This setup isolates the impact of the assimilated ocean state on floe motion and provides a clear baseline for validating the domain-decomposed technique.

The ocean flow field is represented in Fourier space: each mode $\hat{u}_{\mathbf{k},\zeta}$ is modelled as a linear stochastic system, where $\mathbf{k}$ is the 2D wavenumber and ζ indexes mode types associated with the same wavenumber [1, 4, 6, 13]. While the true dynamics involve nonlinear interactions, this linear stochastic approximation is widely used in DA to capture the dominant oscillatory and dissipative behaviour [6, 7], with additive noise parameterising unresolved processes and maintaining ensemble spread for uncertainty quantification. With this in mind, a single Fourier mode is modelled as (see, for example, [25])

$$\frac{d\hat{u}_{\mathbf{k},\zeta}}{dt} = ((-d_{\mathbf{k},\zeta} + i\phi_{\mathbf{k},\zeta})\hat{u}_{\mathbf{k},\zeta} + f_{\mathbf{k},\zeta}) + \sigma_{\mathbf{k},\zeta} dW_{\mathbf{k},\zeta}, \tag{2}$$

where $d_{\mathbf{k},\zeta}$ is the damping coefficient, $\phi_{\mathbf{k},\zeta}$ is the phase speed, $f_{\mathbf{k},\zeta}$ is the external forcing, $\sigma_{\mathbf{k},\zeta}$ is the strength of the stochastic forcing, and $W_{\mathbf{k},\zeta}$ is a complex-valued white noise. Collecting all modes into the spectral state vector $\hat{\mathbf{u}}^o$, the compact representation of the ocean dynamics leads to (1c) where $\mathbf{L^u}$ is the linear operator representing damping and oscillation, $\mathbf{F^u}$ denotes external forcing, and $\mathbf{\Sigma^u} d\mathbf{W^u}$ is the multivariate stochastic forcing. Finally, the ocean velocity field in physical space is reconstructed via the inverse Fourier transform (1c) with $\mathbf{G}(\mathbf{x})$ denoting the inverse Fourier transform operator evaluated on the physical grid.

Despite this idealised setting, there are challenges in simulations, especially when moving toward floes with more features in complex ocean-floe dynamics. First, the computational cost increases rapidly with the number of floes L since advancing the Lagrangian system requires evaluating the ocean velocity at each floe location. Second, the ocean flow field is not directly observed at the spatial and temporal resolutions required to drive floe-scale dynamics; in addition, available observation are often sparse and indirect.

3 Domain-decomposed ocean dynamics data assimilation

To assimilate dense, localised Lagrangian floe observations while recovering a coherent global ocean flow field, we propose a subdomain-based DA strategy. The key idea is to (i) perform ensemble DA independently in each spatial subdomain using only local observations, and then (ii) reconstruct the global ocean field through smooth Gaussian blending.

We partition the original Eulerian domain D into S non-overlapping subdomains $\{A_s\}_{s=1}^{S}$ and process them independently (Algorithm 1). In each A_s, we form a reduced local observation set by selecting L^{obs} representative floes, prioritising those closest to the subdomain centre C_s (and, when applicable, larger floes), which reduces the observation dimension while retaining information most relevant to the local flow. The local state vector for A_s is $[\mathbf{x}_{l^{obs}}, \mathbf{v}_{l^{obs}}, \hat{\mathbf{u}}_s^o]$, where $\mathbf{x}_{l^{obs}}, \mathbf{v}_{l^{obs}}$ are observed floe states and $\hat{\mathbf{u}}_s^o$ are global Fourier coefficients. Given

ICCS Camera Ready Version 2026
To cite this paper please use the final published version:
DOI: 10.1007/978-3-032-29912-3_8

Algorithm 1 Domain-Decomposed Lagrangian DA

Require: Total number of floes L; number of subdomains S; observations per subdomain L^{obs} (with $L \gg S \times L^{\text{obs}}$).

Ensure: Updated local Fourier coefficients $\hat{\mathbf{u}}_s^o$ for each subdomain A_s.

1: Initialise positions and velocities of L floes; Initialise Fourier coefficients for the ocean model
2: Partition the domain into S non-overlapping subdomains $\{A_s\}_{s=1}^{S}$.
3: **for** each subdomain A_s(parallelisable) **do**
4: Compute the geometric centre $\mathbf{C}_s$ of A_s.
5: Select L^{obs} floes within A_s as the local observation set, giving priority to those with larger radii and closer to $\mathbf{C}_s$.
6: **while** assimilation time $t < T$ **do**
7: Assimilate the observed floe positions using ETKF to update the local state vector (floe velocities and local Fourier coefficients $\hat{\mathbf{u}}_s^o$)
8: $t \leftarrow t + \Delta t^{\text{obs}}$
9: **end while**
10: Map $\hat{\mathbf{u}}_s^o$ to physical space to compute the local ocean velocity field $\mathbf{u}_s^o(\mathbf{x})$.
11: Apply a Gaussian weighting function $W_s(\mathbf{x})$ centered on A_s to $\mathbf{u}_s^o(\mathbf{x})$, storing the result for post-analysis fusion.
12: **end for**

the selected observations, each subdomain performs an ETKF analysis to jointly update the local state vector. The updated coefficients are then mapped to physical space to obtain a local velocity field $\mathbf{u}_s^o(\mathbf{x})$ for subsequent Gaussian weighting and cross-subdomain fusion.

To suppress discontinuities across subdomain interfaces, we blend these subdomain fields using a smooth Gaussian weight matrix W_s centred on each subdomain. Assume the domain is D, we decompose this domain uniformly into a grid of size $N^x \times N^y$. The corresponding grid nodes are located at $(x_i, y_j), i = 0, 1, 2, \cdots, N^x, j = 0, 1, 2, \cdots, N^y$. Specifically, we define the normalised weights as

$$W_s^{\text{norm}}(i,j) = \frac{W_s(i,j)}{\sum_{s=1}^{S} W_s(i,j)}, \quad W_s(i,j) = \exp\left(-\frac{(x_i - C_s^x)^2 + (y_j - C_s^y)^2}{2(\sigma^{\text{o}})^2}\right), \tag{3}$$

where (C_s^x, C_s^y) is the centre of subdomain s and σ^o controls the spatial decay. The global ocean velocity field is then reconstructed by Gaussian-weighted fusion:

$$\mathbf{u}^o(x_i, y_j) = \sum_{s=1}^{S} W_s^{\text{norm}}(i,j)\, \mathbf{u}_s^o(x_i, y_j), \tag{4}$$

where $\mathbf{u}^o(x_i, y_j)$ is the nodal value and for an arbitrary point $(x, y) \in D$, $\mathbf{u}^o(x, y)$ is constructed using the bilinear finite element basis as an interpolation. This decomposition reduces the computational burden relative to full-domain assimilation in high-dimensional settings with many floes and Fourier modes, and it is naturally parallelisable because subdomain assimilations are independent.

ICCS Camera Ready Version 2026
To cite this paper please use the final published version:
DOI: 10.1007/978-3-032-29912-3_8

Table 1. Final-time accuracy and runtime by grid size and observation density.

Grid	L^{obs}	NRMSE ↓	PCC ↑	Runtime (10^3 s) ↓
1×1	20	0.90	0.48	4.6
1×1	50	0.91	0.50	5.9
1×1	100	0.70	0.74	7.7
1×1	200	**0.68**	**0.77**	12.0
2×2	10	0.83	0.57	4.6
2×2	20	0.75	0.68	4.3
2×2	50	0.65	0.76	7.5
2×2	100	**0.55**	**0.83**	8.0
4×4	5	0.89	0.62	4.3
4×4	10	0.85	0.67	4.3
4×4	20	0.82	0.68	4.2
4×4	50	**0.74**	**0.74**	5.4

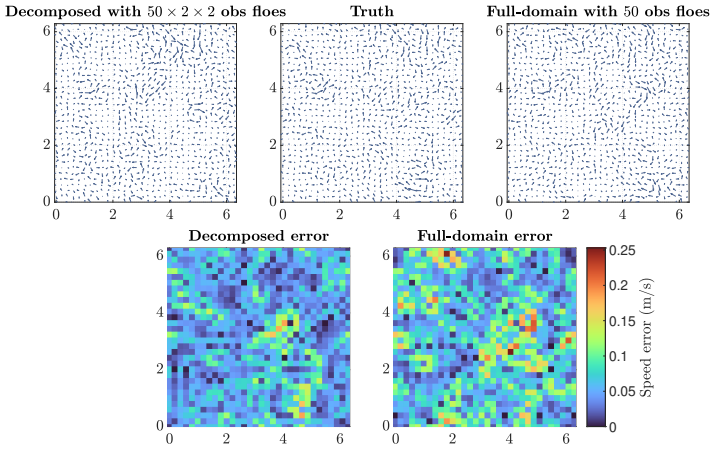

Fig. 1. Ocean velocity-field reconstructions and error distributions at $T = 20$. Top row: velocity fields from the decomposed DA (left), ground truth (middle), and full-domain DA (right). Bottom row: error magnitude maps comparing the decomposed (left) and full-domain (right) reconstructions against the ground truth.

Within each subdomain, ETKF provides an ensemble-space analysis transform, enabling more accurate local updates before global reconstruction.

4 Experimental Results

We consider the dynamics of 40,000 free-drifting floes of unit thickness, with radii sampled from a power-law distribution $N(r) \propto r^{-\alpha}$ with $\alpha = 1.3$. The ocean flow is represented by truncated GB modes with $k_{\max} = 9$; each mode evolves under

ICCS Camera Ready Version 2026
To cite this paper please use the final published version:
DOI: 10.1007/978-3-032-29912-3_8

linear damping and stochastic forcing with coefficients $d = 0.5$ and $\sigma = 0.05$. The DA method is performed using an ETKF with 1000 ensemble members. Observations are noisy floe positions with Gaussian errors (standard deviation 0.01 in non-dimensional units). We set σ^o empirically based on numerical experiments. A small sensitivity check on 2×2 grid indicates that, while larger σ^o values yield a slightly higher PCC ($\sim$0.01 improvements when $\sigma^o = 3.2$), $\sigma^o = 2.6$ provides lower NRMSE value. We remark that alternative reconstruction and smoothing procedures for the ocean field reconstruction could be considered for potentially improved performance but this is not the main focus of this work.

Table 1 summarises results for the 1×1 full-domain baseline and decomposed 2×2 and 4×4 grids, across a range of observation counts L^{obs} (per subdomain). Overall, increasing L^{obs} improves accuracy, with the largest gains from sparse to moderate observation budgets and diminishing returns thereafter. For the baseline, NRMSE decreases from 0.90 ($L^{\text{obs}} = 20$) to 0.70 (100) and 0.68 (200), while PCC increases from 0.48 to 0.74 and 0.77. A similar pattern holds for 2×2: raising L^{obs} from 10 to 50 per subdomain improves NRMSE/PCC from 0.83/0.57 to 0.65/0.76, with smaller additional gains at $L^{\text{obs}} = 100$ (0.55/0.83). For comparable observation budgets, 2×2 consistently outperforms 4×4 at the final time, suggesting that finer partitioning becomes information-constrained under current tuning: smaller subdomains capture cross-boundary correlations less effectively and local updates recover large-scale coherence less well. Relative to 1×1, the 2×2 setting can match or exceed accuracy with fewer observations.

If the grid is further refined (larger S), each subdomain contains fewer floes; with a fixed L^{obs} the selected representative floes are more likely to lie near subdomain interfaces and be influenced by flow structures extending into neighbouring subdomains. Although Gaussian-weighted blending mitigates some boundary inconsistencies, it cannot fully recover missing cross-subdomain information, which may limit further accuracy gains for finer partitions. Increasing L^{obs} also substantially raises computational cost, since drag forcing must be computed for more floes at each time step.

All wall-clock runtimes range from $\sim 4.2 \times 10^3$ to 1.2×10^4 s and increase with L^{obs}. Decomposition can achieve similar or higher accuracy at lower cost; for example, with 200 floes observed, 2×2 with $L^{\text{obs}} = 50$ attains NRMSE/PCC $= 0.65/0.76$ in 7.5×10^3 s, compared with 0.68/0.77 in 1.2×10^4 s for 1×1.

To complement these statistics, we next visualise a representative snapshot of the reconstructed flow field. Fig. 1 compares the velocity-field reconstruction at day 20 for decomposed and full-domain DA. The decomposed method aligns closer to the ground truth, particularly in preserving localised circulation features. The corresponding error-magnitude maps confirm this improvement, with fewer high-error regions and reduced error magnitudes in the decomposed case.

5 Conclusions

In this paper, we developed a domain-decomposed DA framework for multi-scale ocean field recovery in sea-ice modelling that consistently outperforms a

ICCS Camera Ready Version 2026
To cite this paper please use the final published version:
DOI: 10.1007/978-3-032-29912-3_8

full-domain baseline across key metrics. These improvements arise from three synergistic mechanisms: (1) each subdomain provides a finer-scale ocean recovery (high-frequency modes) of the floe field; (2) as the subdomains are independent, their updates can be computed in parallel; and (3) Gaussian-weighted blending keeps large-scale flow structures smooth while damping noise at subdomains. As further work, one direction is to extend the framework to fully coupled DEM configurations with floe rotations and floe-floe contact mechanics. In such settings, we expect the domain-decomposed analysis to be more advantageous because contact-induced stresses and deformation are strongly localised in space, performing inference within subdomains may better preserve these local interactions while maintaining global consistency through blending.

Acknowledgments. This research was undertaken with the assistance of resources from the National Computational Infrastructure (NCI Australia) under grants zv32 and um09. The authors acknowledge the support of the Australian National University, and Q.D. acknowledges support from start-up funding provided by the Yau Mathematical Sciences Center, Tsinghua University.

References

1. Berner, J., Achatz, U., Batte, L., Bengtsson, L., Cámara, A.d.l., Christensen, H.M., Colangeli, M., Coleman, D.R., Crommelin, D., Dolaptchiev, S.I., et al.: Stochastic parameterization: Toward a new view of weather and climate models. Bulletin of the American Meteorological Society **98**(3), 565–588 (2017)
2. Bishop, C.H., Etherton, B.J., Majumdar, S.J.: Adaptive sampling with the ensemble transform Kalman filter. Part I: Theoretical aspects. Monthly weather review **129**(3), 420–436 (2001)
3. Bouillon, S., Fichefet, T., Legat, V., Madec, G.: The elastic–viscous–plastic method revisited. Ocean Modelling **71**, 2–12 (2013)
4. Branicki, M., Majda, A.J., Law, K.J.: Accuracy of some approximate Gaussian filters for the Navier–Stokes equation in the presence of model error. Multiscale Modeling & Simulation **16**(4), 1756–1794 (2018)
5. Cavalieri, D.J., Parkinson, C.L.: Arctic sea ice variability and trends, 1979–2010. The Cryosphere **6**(4), 881–889 (2012)
6. Chen, N., Deng, Q., Stechmann, S.N.: Superfloe parameterization with physics constraints for uncertainty quantification of sea ice floes. SIAM/ASA Journal on Uncertainty Quantification **10**(4), 1384–1409 (2022)
7. Chen, N., Fu, S., Manucharyan, G.: Lagrangian data assimilation and parameter estimation of an idealized sea ice discrete element model. Journal of Advances in Modeling Earth Systems **13**(10), e2021MS002513 (2021)
8. Comiso, J.C., Parkinson, C.L., Gersten, R., Stock, L.: Accelerated decline in the Arctic sea ice cover. Geophysical research letters **35**(1) (2008)
9. Damsgaard, A., Adcroft, A., Sergienko, O.: Application of discrete element methods to approximate sea ice dynamics. Journal of Advances in Modeling Earth Systems **10**(9), 2228–2244 (2018)
10. Deng, Q., Chen, N., Stechmann, S.N., Hu, J.: LEMDA: A Lagrangian-Eulerian multiscale data assimilation framework. Journal of Advances in Modeling Earth Systems **17**(2), e2024MS004259 (2025)

ICCS Camera Ready Version 2026
To cite this paper please use the final published version:
DOI: 10.1007/978-3-032-29912-3_8

11. Dolean, V., Jolivet, P., Nataf, F.: An introduction to domain decomposition methods: algorithms, theory, and parallel implementation. SIAM (2015)
12. Evensen, G.: The ensemble Kalman filter: Theoretical formulation and practical implementation. Ocean dynamics **53**, 343–367 (2003)
13. Farrell, B.F., Ioannou, P.J.: Stochastic forcing of the linearized Navier–Stokes equations. Physics of Fluids A: Fluid Dynamics **5**(11), 2600–2609 (1993)
14. Feltham, D.L.: Sea ice rheology. Annu. Rev. Fluid Mech. **40**(1), 91–112 (2008)
15. Herman, A.: Discrete-Element bonded-particle Sea Ice model DESIgn, version 1.3 a–model description and implementation. Geoscientific Model Development **9**(3), 1219–1241 (2016)
16. Hibler III, W.: A dynamic thermodynamic sea ice model. Journal of physical oceanography **9**(4), 815–846 (1979)
17. Hopkins, M.A.: A discrete element Lagrangian sea ice model. Engineering Computations **21**(2/3/4), 409–421 (2004)
18. Hunke, E.C.: Viscous–plastic sea ice dynamics with the EVP model: Linearization issues. Journal of Computational Physics **170**(1), 18–38 (2001)
19. Hunt, B.R., Kostelich, E.J., Szunyogh, I.: Efficient data assimilation for spatiotemporal chaos: A local ensemble transform Kalman filter. Physica D: Nonlinear Phenomena **230**(1-2), 112–126 (2007)
20. Junior, R.A.A., Mellado-Cusicahua, A., Shakibaeinia, A., Cheng, L.Y.: A fully Lagrangian DEM-MPS mesh-free model for ice-wave dynamics. Cold Regions Science and Technology **186**, 103266 (2021)
21. Kelman, I.: Arcticness: Power and Voice from the North. UCL Press (2017)
22. Kelman, I.: Antarcticness: Inspirations and Imaginaries. UCL Press (2022)
23. Law, K., Stuart, A., Zygalakis, K.: Data assimilation. Cham, Switzerland: Springer **214**, 52 (2015)
24. Lemieux, J.F., Tremblay, B.: Numerical convergence of viscous-plastic sea ice models. Journal of Geophysical Research: Oceans **114**(C5) (2009)
25. Majda, A., Wang, X.: Nonlinear dynamics and statistical theories for basic geophysical flows. Cambridge University Press (2006)
26. Meier, W.N., Stroeve, J., Fetterer, F.: Whither Arctic sea ice? A clear signal of decline regionally, seasonally and extending beyond the satellite record. Annals of Glaciology **46**, 428–434 (2007)
27. Neal, J.C., Atkinson, P.M., Hutton, C.W.: Evaluating the utility of the ensemble transform Kalman filter for adaptive sampling when updating a hydrodynamic model. Journal of hydrology **375**(3-4), 589–600 (2009)
28. Nino-Ruiz, E.D., Sandu, A., Deng, X.: A parallel implementation of the ensemble Kalman filter based on modified Cholesky decomposition. Journal of Computational Science **36**, 100654 (2019)
29. Quarteroni, A., Valli, A.: Domain decomposition methods for partial differential equations. Oxford University Press (1999)
30. Rampal, P., Weiss, J., Marsan, D.: Positive trend in the mean speed and deformation rate of Arctic sea ice, 1979–2007. Journal of Geophysical Research: Oceans **114**(C5) (2009)
31. Serreze, M.C., Holland, M.M., Stroeve, J.: Perspectives on the Arctic's shrinking sea-ice cover. science **315**(5818), 1533–1536 (2007)
32. Thomas, D.N., Dieckmann, G.S.: Sea ice: an introduction to its physics, chemistry, biology and geology. John Wiley & Sons (2008)
33. Toselli, A., Widlund, O.: Domain decomposition methods-algorithms and theory, vol. 34. Springer Science & Business Media (2004)

ICCS Camera Ready Version 2026
To cite this paper please use the final published version:
DOI: 10.1007/978-3-032-29912-3_8